Current Biology 24, 1421–1428, June 16, 2014 ©2014 Elsevier Ltd All rights reserved http://dx.doi.org/10.1016/j.cub.2014.05.019

Report

An Arp2/3 Nucleated F-Actin Shell Fragments Nuclear Membranes at Nuclear Envelope Breakdown in Starfish Oocytes

Masashi Mori,[1] Kálmán Somogyi,[1] Hiroshi Kondo,[1] Nilah Monnier,[3,4] Henning J. Falk,[1] Pedro Machado,[2] Mark Bathe,[3,5] François Nédélec,[1] and Péter Lénárt[1,*]

[1]Cell Biology and Biophysics Unit
[2]Electron Microscopy Core Facility
European Molecular Biology Laboratory (EMBL), Meyerhofstrasse 1, Heidelberg 69117, Germany
[3]Laboratory for Computational Biology and Biophysics, Department of Biological Engineering, Massachusetts Institute of Technology (MIT), 77 Massachusetts Avenue, Cambridge, MA 02139, USA
[4]Graduate Program in Biophysics, Harvard University, 1350 Massachusetts Avenue, Cambridge, MA 02138, USA
[5]Broad Institute of MIT and Harvard, 301 Binney Street, Cambridge, MA 02142, USA

Summary

Animal cells disassemble and reassemble their nuclear envelopes (NEs) upon each division [1, 2]. Nuclear envelope breakdown (NEBD) serves as a major regulatory mechanism by which mixing of cytoplasmic and nuclear compartments drives the complete reorganization of cellular architecture, committing the cell for division [2, 3]. Breakdown is initiated by phosphorylation-driven partial disassembly of the nuclear pore complexes (NPCs), increasing their permeability but leaving the overall NE structure intact [4–7]. Subsequently, the NE is rapidly broken into membrane fragments, defining the transition from prophase to prometaphase and resulting in complete mixing of cyto- and nucleoplasm [6, 8]. However, the mechanism underlying this rapid NE fragmentation remains largely unknown. Here, we show that NE fragmentation during NEBD in starfish oocytes is driven by an Arp2/3 complex-nucleated F-actin "shell" that transiently polymerizes on the inner surface of the NE. Blocking the formation of this F-actin shell prevents membrane fragmentation and delays entry of large cytoplasmic molecules into the nucleus. We observe spike-like protrusions extending from the F-actin shell that appear to "pierce" the NE during the fragmentation process. Finally, we show that NE fragmentation is essential for successful reproduction, because blocking this process in meiosis leads to formation of aneuploid eggs.

Results and Discussion

An F-Actin Shell Polymerizes Transiently Underneath the NE at NEBD

Although fragmentation of the nuclear envelope (NE) has been studied in various model organisms and has been proposed to have important functions in cell division, the mechanisms that drive NE fragmentation during nuclear envelope breakdown (NEBD) remain poorly understood [1, 2]. In mammalian fibroblasts, centrosomal microtubules tear open and remove the NE from the nuclear surface [8, 9], but it is unclear to what extent this process contributes to actual membrane fragmentation. Importantly, such a microtubule-driven mechanism is unlikely to be sufficient in cell types like large oocytes with disproportionately large nuclei compared to the size of microtubule asters. Indeed, NE fragmentation is known to be independent of microtubules in starfish oocytes [6], clearly requiring the existence of alternative mechanisms. In previous studies, we noted a bright, dense, and transient shell of F-actin of unknown function that polymerizes along the NE around the time of NEBD in starfish oocytes [10]. The temporal and spatial proximity of this F-actin shell to NE fragmentation suggested that it may play a role in promoting fragmentation.

Using fast 3D imaging, we find that the F-actin shell initiates at a few individual foci on the NE and then rapidly spreads to engulf the entire nucleus in ~1 min (Figure 1A). This F-actin shell can be observed along the NE by a variety of live-cell F-actin markers and by phalloidin staining in fixed cells (Figures 1A–1D) [10]. High-resolution light microscopy confirms previous findings by immunogold electron microscopy (EM) [10] that the F-actin shell forms on the inner, nuclear side of the NE (Figure 1E). The F-actin shell then depolymerizes in ~1 min (Figure 1A), with the exception of dense patches of F-actin surrounding chromosomes close to the nuclear periphery (Figures S1A–S1E available online). The shell forms concomitantly with the network of F-actin bundles in the nuclear region that we have shown previously to drive chromosome congression [10, 13] but that is distinct in structure and molecular composition (Figures S1F and S1G).

The F-Actin Shell Is Nucleated by the Arp2/3 Complex

Based on the dense morphology of the F-actin shell, we hypothesized that the Arp2/3 complex might be involved in its nucleation. Indeed, we observe specific localization of mEGFP-tagged Arpc1, a subunit of the Arp2/3 complex, to the F-actin shell, but not to the F-actin bundle network (Figure 1F). This localization is confirmed by immunofluorescence labeling with an anti-Arpc1 antibody (Figure S1H). Consistent with Arpc1 localization, we find that treatment of oocytes with the small-molecule Arp2/3 inhibitor CK-666, but not its inactive analog, CK-689 [14], abolishes formation of the F-actin shell, but does not prevent formation of the bundle network (Figures 1G–1I and S1I and Movie S1). Many CK-666-treated oocytes still retain small remnants of F-actin foci along the NE at NEBD, but these foci do not spread into a full F-actin shell (Figures 1G and 1H). These remnants most likely result from incomplete inhibition of Arp2/3, due to the relatively low affinity of CK-666 [14]. To quantify our observations of shell inhibition, we measured mean F-actin fluorescence intensity along the nuclear rim, and we found that CK-666 effectively blocks the transient enrichment of F-actin in the rim region that is seen in DMSO-treated control oocytes (Figure 1I). Together, these data indicate that the Arp2/3 complex is required specifically to nucleate the F-actin shell, but not the F-actin bundle network, during NEBD.

The F-Actin Shell Is Required for Timely and Complete Permeabilization of the NE

Previous studies of NEBD in starfish oocytes have shown that NE fragmentation begins at a single or few foci and then rapidly

*Correspondence: lenart@embl.de

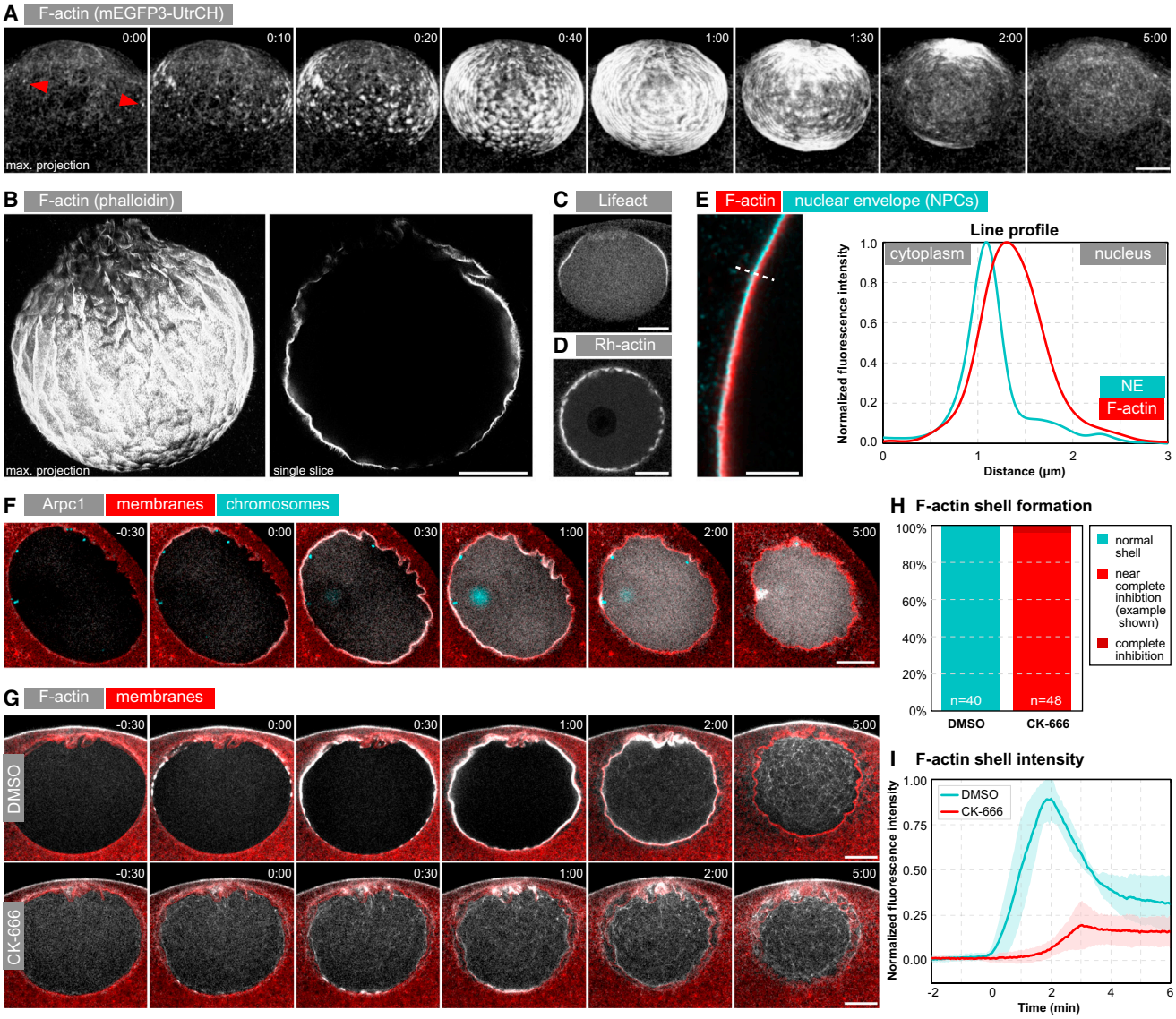

Figure 1. An Arp2/3-Nucleated F-actin Shell Forms Transiently along the NE at NEBD in Starfish Oocytes

(A) Maximum-intensity z projections of the nuclear region of a live oocyte expressing mEGFP3-UtrCH (the calponin homology domain of human utrophin protein tagged with three mEGFPs [11]) to visualize the formation, spreading, and disassembly of the F-actin shell. The cell cortex has been segmented out to allow visualization of the cell interior. Times are shown relative to the start of NEBD. Red arrowheads mark initial F-actin foci.

(B) Partially formed F-actin shell in an oocyte fixed during NEBD and stained with Alexa 488-phalloidin. A maximum-intensity z projection of the entire nuclear region (left) and a selected single confocal section (right) are shown.

(C) Single confocal section through a partially formed F-actin shell labeled by the Lifeact-EGFP F-actin marker [12] in a live oocyte.

(D) Single confocal section through an almost fully formed F-actin shell labeled by rhodamine-actin in a live oocyte.

(E) Left: deconvolved confocal section through the NE of an oocyte fixed during NEBD and stained with mAb414 to label NPCs (cyan) and Alexa 568-phalloidin to label the F-actin shell (red). Right: intensity profile for the two channels along the dashed line marked on the image at left.

(F) Confocal sections through the nuclear region of a live oocyte expressing the Arp2/3 complex subunit mEGFP-Arpc1 (gray) and injected with $DiIC_{18(3)}$ to label membranes (red) and histone H1-Alexa647 to label chromosomes and also the nucleolus (cyan), revealing specific recruitment of Arpc1 to the F-actin shell.

(G) Confocal sections through the nuclear regions of live oocytes expressing mEGFP3-UtrCH (gray) and injected with $DiIC_{18(3)}$ (red), incubated for 1 hr with either 0.5 mM CK-666 or a corresponding amount of DMSO prior to NEBD.

(H) Fraction of oocytes with complete or near-complete inhibition of the F-actin shell for the CK-666 versus DMSO treatment conditions as in (G). Oocytes were scored for the presence or absence of the F-actin shell, and n is the number of oocytes imaged in each condition.

(I) Mean F-actin intensity along the NE measured from time-lapse recordings such as those shown in (G). The NE was automatically segmented by thresholding of the $DiIC_{18(3)}$ channel at each time point. Mean mEGFP3-UtrCH intensity measurements along the segmented NE were normalized such that control oocytes ranged from 0 to 1. Averages (solid lines) and SDs (shaded regions) of the normalized mean intensity are shown for five oocytes each for both CK-666 and DMSO treatment.

Times are given as min:s relative to NEBD. Scale bars represent 20 µm (A–D and G) and 5 µm (E). See also Figure S1 and Movie S1.

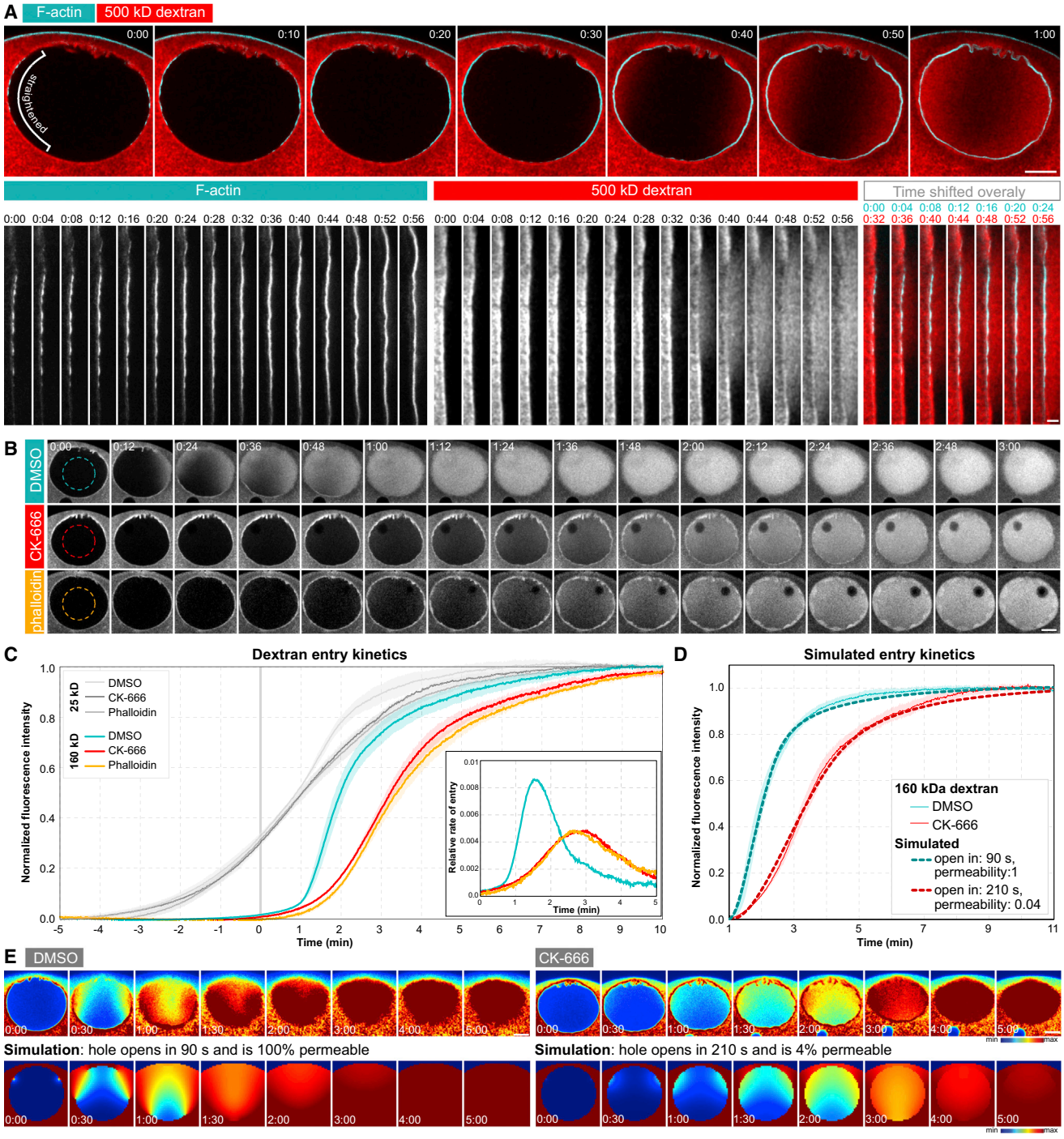

Figure 2. The F-Actin Shell Is Required for Timely and Complete Permeabilization of the NE

(A) Top: confocal sections through the nuclear region of a live oocyte expressing mEGFP3-UtrCH (cyan) and injected with Cy5-labeled 500 kD dextran (red) showing the tight spatial and temporal correlation between F-actin shell formation and dextran entry. Bottom: mEGFP3-UtrCH and 500 kD dextran intensity along a portion of the NE (as marked on the leftmost image above), shown "unrolled" into a straight line. On the far right is an overlay of the mEGFP3-UtrCH and dextran channels with a 32 s time shift to highlight the precise spatial correlation between F-actin shell formation and dextran entry.

(B) Confocal sections through the nuclear region of live oocytes coinjected with Cy5-lableled 25 and TRITC-labeled 160 kD dextrans and either incubated with DMSO or CK-666 or injected with an excess of phalloidin prior to NEBD. The 160 kD dextran channel is shown, demonstrating the delay in dextran entry upon interference with F-actin shell formation.

(C) Quantification of mean nuclear fluorescence intensity (measured within the dashed circles shown in B) for the 25 and 160 kD dextran channels (gray and colored lines, respectively) for oocytes treated with DMSO or CK-666 or injected with phalloidin as shown in (B). Averages (solid lines) and SDs (shaded regions) of mean intensity from at least five oocytes are shown. The mean intensity values are normalized for each condition by defining zero as the mean of the measurements between −5 and −4 min and one as the mean of the measurements between 9 and 11 min. The inset shows the rate of change of the mean nuclear fluorescence intensity, reflecting the rate of dextran entry into the nuclear region, calculated using a moving average of ten frames.

(legend continued on next page)

spreads from these locations along the NE. This pattern of NE fragmentation can be inferred from the kinetics of entry of large cytoplasmic molecules into the nuclear region [7] and directly visualized by fast imaging of live oocytes and by electron microscopy [6]. Although polymerization of the F-actin shell along the NE occurs at roughly the same time as NE fragmentation, earlier data did not allow us to dissect the temporal order of these events [10]. Using improved markers and imaging conditions, here we find that the earliest F-actin foci form ~30 s before the entry of large cytoplasmic molecules (160 or 500 kD dextrans) into the nuclear region (Figure 2A and Movie S2). This temporal offset rules out the possibility that the shell forms as a consequence of NE fragmentation. Subsequently, as the F-actin foci spread along the NE and merge into a continuous shell, dextran entry begins exactly at the site where the foci first appeared and spreads in the same pattern as the F-actin shell, continuing to lag the shell by ~30 s (Figure 2A).

To test whether there is a causal relationship between these two processes, as suggested by their tight spatiotemporal correlation, we followed the kinetics of dextran entry in oocytes treated with CK-666 to block formation of the F-actin shell (Figures 2B and 2C). Previous studies have shown that initial entry of small (25 kD) dextran occurs via nuclear pore complex (NPC) disassembly early in NEBD, when nuclear membranes are still intact, while entry of large (160 or 500 kD) dextran requires NE fragmentation [6]. As expected, the initial entry kinetics of 25 kD dextran through NPCs prior to membrane fragmentation are not affected by CK-666 treatment (Figure 2C, −5 to 0 min, gray lines), confirming that the F-actin shell and Arp2/3 complex are not involved in NPC disassembly, which is driven by phosphorylation of nucleoporins [5]. In contrast, entry of 160 kD dextran is considerably delayed in CK-666 treated oocytes (Figures 2B and 2C, colored lines; Movie S2), implying a role for the F-actin shell in NE fragmentation. Interestingly, it is the rate of entry rather than the start time of entry that is affected, with a roughly 2-fold reduction in the peak entry rate (Figure 2C, inset). To exclude any nonspecific effects of CK-666, we confirmed this delay in dextran entry in oocytes treated with cytochalasin D or latrunculin B to prevent actin polymerization altogether (Figure S2A). Finally, because those drugs may have side effects that damage the cell cortex, we also injected excess phalloidin into oocytes prior to NEBD to drive all cellular actin into stabilized cytoplasmic filament bundles and thereby prevent formation of any new F-actin structures without damaging the cell cortex. Phalloidin injection effectively blocks F-actin shell formation (data not shown) and delays entry of the 160 kD dextran in a manner indistinguishable from CK-666 treatment (Figures 2B and 2C).

To explore how the observed change in dextran entry kinetics could be caused by altered properties of NE fragmentation in the absence of the F-actin shell, we performed quantitative simulations of dextran entry using a model previously developed by Terasaki et al. [7] in which a spherical NE contains an area of permeabilization (fragmentation) that can vary in size and permeability to diffusing dextran molecules (Figure S2B). We defined the initiation site and growth rate of the permeabilization area based on experimental observations and fit the diffusion coefficient of the dextran molecules to match the entry kinetics observed in control oocytes [6]. With these parameters, the model closely reproduces the experimentally observed spatial and temporal kinetics of dextran entry in control oocytes (Figures 2D and 2E). In this model, a delay in dextran entry could be caused by a reduction either in the rate at which the area of permeabilization grows over time or in its permeability to dextran. We found that the best fit to the delayed dextran entry kinetics observed in oocytes treated with CK-666 is obtained when the speed of spreading is reduced by 2.3-fold and the permeability is reduced by 25-fold (Figures 2D, 2E, and S2C).

Taken together, these dextran results indicate that formation of the transient F-actin shell, as mediated by Arp2/3, is required for efficient fragmentation of the NE at NEBD; in the absence of the F-actin shell, the NE remains largely intact. This reduction in permeability could be caused by a failure of initial breakpoints in the NE to expand and efficiently fragment NE membranes, consistent with our observation that only the rate of dextran entry, and not the start time of entry, is affected by treatment with CK-666.

Inhibition of the F-Actin Shell Leaves the NE Intact after NEBD

As NE fragmentation can be resolved by electron microscopy (EM) [6], we sought to directly visualize fragmentation in the presence and absence of the F-actin shell. To support these data with larger sample numbers, we additionally developed a light-microscopy fragmentation assay based on immunostaining of NPCs in fixed oocytes. Unlike in somatic cells, the NE of oocytes is tightly packed with NPCs, which form a dense array with ~150 nm spacing (Figure 3A). Therefore, the intact NE before NEBD appears in deconvolved light-microscopy images as a homogeneous grainy surface and a thin continuous line in cross-section (Figure 3B). In contrast, the fragmented NE after NEBD appears in cross-section as a broader fragmented line by light microscopy, consistent with the NE fragments visualized in cross-section by EM (compare Figure 3A with Figure 3B). The surface view of the NE after NEBD in deconvolved light-microscopy images reveals a network of NE fragments (Figure 3B), as was presumed, but not yet directly reconstructed, from thin-section EM data.

In stark contrast to control oocytes, in oocytes treated with CK-666 we observe that the NE remains intact after NEBD by both EM and NPC staining (Figure 3C). These intact NE membranes are observed for more than 20 min after NEBD (Figure 3C, "late stage"). The occurrence of NEBD was confirmed in these samples by the disappearance of the smooth and sharp NE boundary in transmitted light microscopy and the folded morphology of the NE apparent by EM and by costaining the F-actin bundle network in the nuclear region by fluorescence microscopy (Figure 3C). To quantify NE fragmentation, we traced NE fragments on large EM montages of the entire nuclear region after NEBD (Figures 3D and S3), and we found a 25-fold difference in average fragment length of 1.40 ± 0.17 μm in DMSO control (n = 5 oocytes) compared to

(D) Simulated dextran entry kinetics (dashed lines) compared to experimentally measured entry kinetics (thin solid lines with standard deviations) of the 160 kD dextran for CK-666- and DMSO-treated oocytes (same data as C except renormalized between 1 and 11 min).
(E) Comparison of the spatial pattern of 160 kD dextran entry for experiments (top) versus simulation (bottom) for the CK-666- and DMSO-treated oocytes as in (B). Times are shown relative to the initiation of F-actin shell formation in min:s. Scale bars represent 20 μm (A, top; B; and E) and 5 μm (A, bottom). See also Figure S2 and Movie S2.

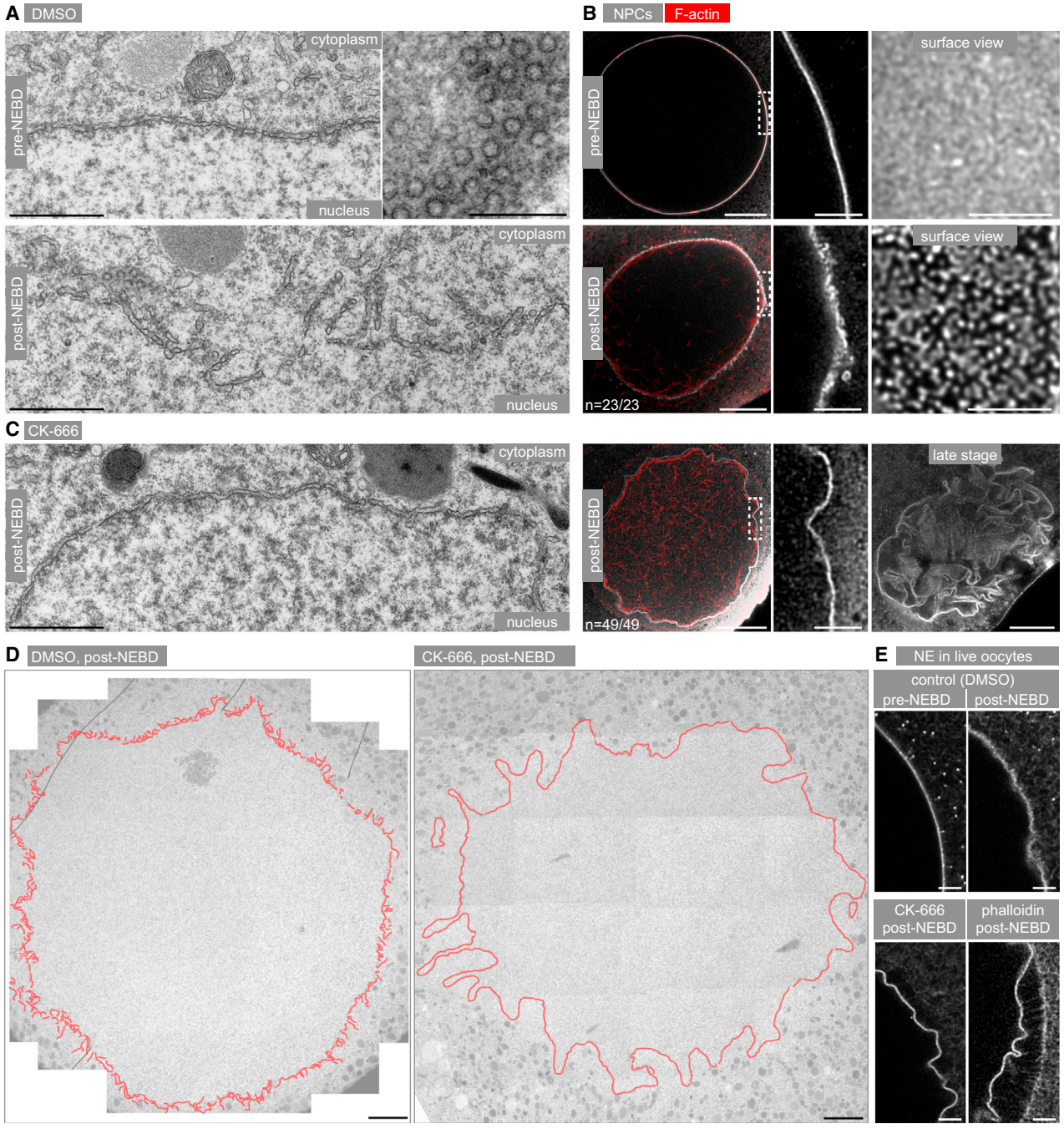

Figure 3. Preventing F-Actin Shell Formation Leaves the NE Intact

(A) Thin-section electron micrographs of the NE in an oocyte fixed before NEBD (top) and an oocyte fixed approximately 3–5 min after NEBD (bottom) visualizing NE fragmentation during NEBD. The inset shows a surface view of the NE tightly packed with NPCs. Scale bars represent 1 μm (top-left and bottom images) or 0.5 μm (top-right image).

(B) Fluorescent staining of the NE by mAb414 (gray) and F-actin by phalloidin (red) in an oocyte fixed before NEBD (top row) and an oocyte fixed after NEBD (bottom row), visualizing NE fragmentation by light microscopy. Left column: single confocal sections of the nuclear region from deconvolved 3D data sets. Middle column: enlarged view of the NE (corresponding to the dashed rectangles at left). Right column: enlarged surface view of the NE taken from a confocal section at the bottom of the nuclear region. Scale bars represent 20 μm (left column) or 5 μm (middle and right columns).

(C) Electron micrograph and immunostaining of the NE after NEBD in oocytes treated with CK-666. Samples were processed together with the control samples shown in (A) and (B). The rightmost image shows an oocyte treated with CK-666 and fixed approximately 20 min after NEBD. Scale bars are as in (A) and (B).

(D) Thin-section EM montage of the entire nuclear region of oocytes fixed after NEBD and treated with CK-666 (right) or a corresponding concentration of DMSO (left). Traced NE fragments are shown in red overlay. Scale bars represent 5 μm.

(E) Single confocal sections through a portion of the nuclear region of live oocytes expressing the nucleoporin POM121-EGFP3 to label the NE. Sections are shown before and after NEBD for an oocyte incubated with DMSO (top) and after NEBD for oocytes incubated with CK-666 or injected with an excess of phalloidin (bottom). Scale bars represent 5 μm.

See also Figure S3 for the raw EM images from (D).

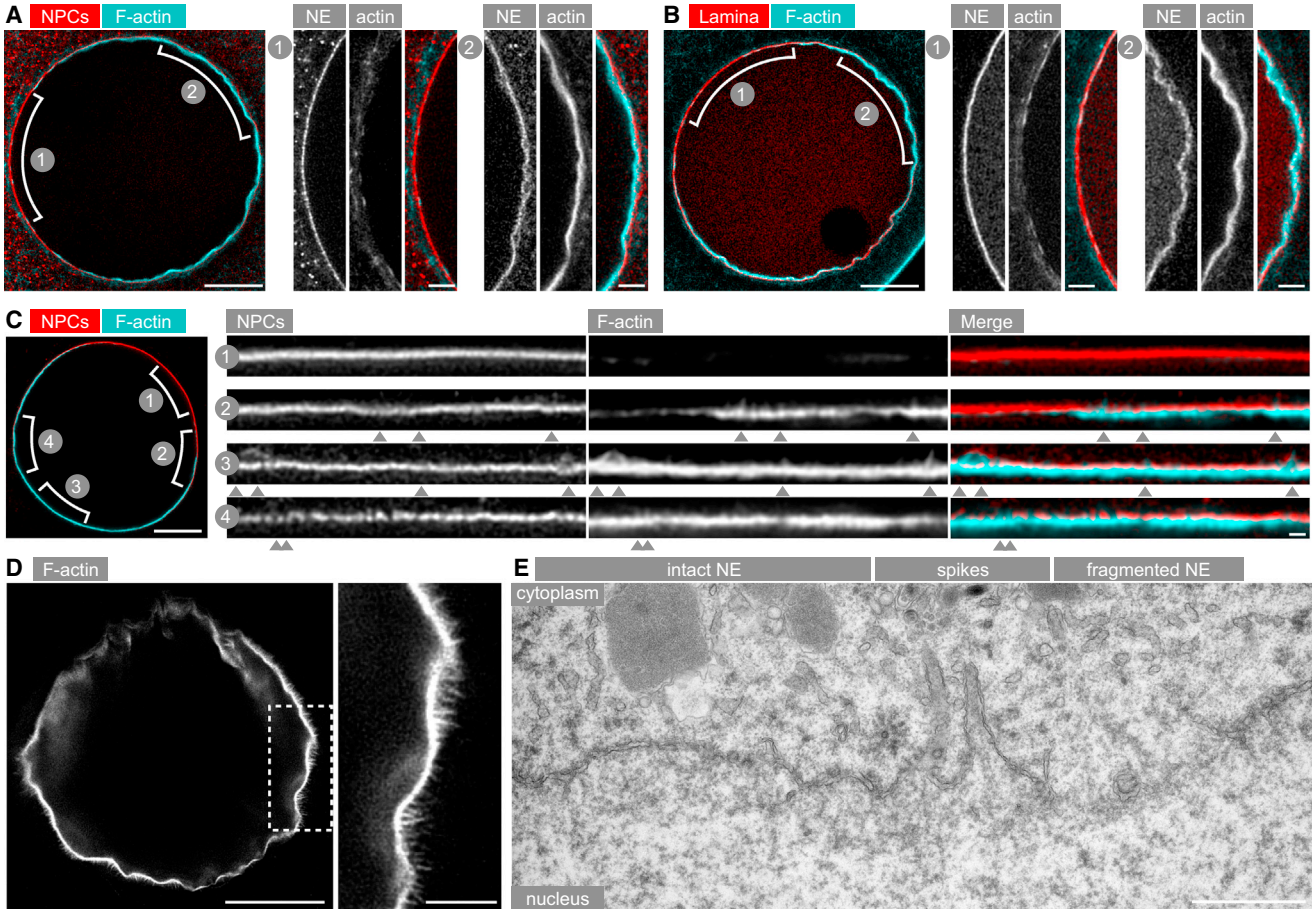

Figure 4. The F-Actin Shell Fragments Nuclear Membranes at NEBD

(A) Deconvolved confocal section of the nuclear region of an oocyte expressing POM121-EGFP3 (red) and mEGFP3-UtrCH (cyan) during formation of the F-actin shell, revealing the tight correlation between the presence of the F-actin shell and fragmentation of the adjacent NE. Enlarged regions of the NE, as marked on the leftmost image (numbers), are shown at right for each channel and as an overlay. Scale bars represent 20 and 5 μm for the overview and enlarged regions, respectively.

(B) Same as (A) for an oocyte expressing lamin B-EGFP instead of POM121-EGFP3 to label the NE.

(C) Fluorescent staining of the NE by mAb414 (red) and F-actin by Alexa 568-phalloidin (cyan) in an oocyte fixed during formation of the F-actin shell. Enlarged regions of the NE, as marked on the leftmost image (numbers), are shown at right "unrolled" into straight lines. Arrowheads highlight prominent spike-like protrusions of the F-actin shell. Scale bars represent 20 and 1 μm for the overview and enlarged regions, respectively.

(D) Phalloidin staining of an oocyte fixed during formation of the F-actin shell with a buffer optimized to preserve F-actin. A single confocal section from a deconvolved 3D data set is shown (left), along with an enlarged view of the NE (right). Scale bars represent 20 and 5 μm for the overview and enlarged regions, respectively.

(E) Thin-section electron micrograph of an oocyte fixed during fragmentation of the NE showing spike-like protrusions of the NE at the boundary between intact (left) and fragmented (right) sections of the NE. The scale bar represents 1 μm.

See also Figure S4.

35.51 ± 28.86 μm in CK-666-treated oocytes (n = 4 oocytes). Although these parameters are measured on 2D thin sections and are not directly interpretable in terms of 3D structure, they provide clear evidence for a large difference in membrane morphology in the absence of the F-actin shell. Finally, we confirmed these results in live cells by labeling the NE with the nucleoporin POM121-EGFP3 (Figure 3E). In live CK-666-treated or phalloidin-injected oocytes, the NE boundary remains a thin and continuous line after NEBD that is clearly separated from the bulk endoplasmic reticulum, in contrast to control oocytes in which the broadening and roughening of the NE boundary after NEBD is clearly observed (Figure 3E). Identical observations were made in oocytes treated with cytochalasin D or latrunculin B (Figure S2). Therefore, direct observation of the NE in both live and fixed cells indicates that blocking formation of the F-actin shell prevents NE fragmentation during NEBD.

The F-Actin Shell Fragments Nuclear Membranes at NEBD

Finally, we combined this live-cell NE fragmentation assay with F-actin colabeling in order to directly determine when and where NE fragmentation occurs relative to formation of the F-actin shell. Individual frames of live-cell recordings capture the process of spreading of the F-actin shell, and these frames contain both intact and fragmented portions of the NE as visualized by both NPC and lamina (lamin B-EGFP) markers (Figures 4A and 4B). We observe that the NE is consistently intact in regions where the F-actin shell is not yet present, whereas regions of the NE underlined by the F-actin shell appear fragmented (Figures 4A and 4B). These results indicate that

fragmentation of the NE is rapid and is tightly correlated in space and time with F-actin shell formation. Fixed oocytes with partially formed F-actin shells confirm that fragmentation is spatially correlated with the presence of the F-actin shell (Figure 4C). With the high spatial resolution of these fixed samples, we also observe spike-like F-actin structures, similar in morphology to filopodia, that protrude from the F-actin shell and appear to project through the NE (Figure 4C, arrowheads). These structures are even more prominent in cells fixed in a buffer optimized to preserve F-actin (Figure 4D). To determine whether these F-actin projections might affect NE morphology, we examined the NE in detail in EM samples fixed during this shell-formation stage. We observe very unusual spike-like protrusions of the NE (Figure 4E) that are fully consistent in size and number with the F-actin protrusions visualized by light microscopy. Interestingly, these protrusions are specifically localized to portions of the NE that are still intact but adjacent to fragmented regions (Figure 4E), suggesting that they relate to the mechanism by which fragmentation spreads along the NE.

Conclusions

In conclusion, we have revealed a novel mechanism of NE fragmentation during NEBD that is mediated by an Arp2/3-nucleated shell of F-actin. This F-actin shell spreads along the NE concurrently with visible fragmentation of the NE and its permeabilization to large molecules. The shell is not involved in initial permeabilization, because entry of large dextrans begins at the same time in both control oocytes and oocytes in which shell formation is blocked. However, the rate of entry is significantly reduced in the absence of the F-actin shell, indicating that the shell is required for the rapid spread of NE fragmentation that quickly and completely permeabilizes the NE. In analogy to a dam on a river, the downstream area can be flooded either slowly through small leaks or rapidly by a massive breach. The F-actin shell is required to convert initial leaks in the NE into a massive breach. These initial leaks are believed to form when the core NPC structure disassembles [6, 7]. We hypothesize that these leaks allow cytoplasmic Arp2/3 complexes to enter the nucleus and nucleate the initial foci of F-actin seen along the NE (Figure 1A, arrowheads). These initial foci rapidly grow and spread along the NE through the self-amplifying mechanism of Arp2/3 [15, 16], forming a complete F-actin shell that drives massive fragmentation of the NE by a mechanism that likely involves the spike-like protrusions that we observe to pierce the NE. Although we have shown that Arp2/3 is the major nucleator involved in shell formation, our present data do not exclude the possibility that additional nucleators and other actin regulators associate with the F-actin shell, in a manner similar to lamellipodia formation [17]. Indeed, the long and bundled appearance of the spike-like protrusions suggests the involvement of filament crosslinkers and straight filament nucleators.

In somatic cells, it is widely accepted that rapid breakdown and removal of the NE from the nuclear surface at NEBD is important to allow timely progression of cell division, because intact nuclear membranes physically hinder cytoplasmic microtubules from gaining access to chromosomes [8]. Here we find that inefficient NE fragmentation in the absence of the F-actin shell has a dramatic effect on chromosome congression, with over 70% of CK-666-treated oocytes failing to collect all chromosomes to the meiotic spindle by anaphase onset, leading to the formation of aneuploid eggs (Figure S4 and Movie S3). Thus, rapid and complete fragmentation of the NE is essential for normal progression through meiosis in oocytes as much as for mitosis in somatic cells. It is, however, unclear at present how broadly this F-actin-driven mechanism of NE fragmentation is conserved across species and cell types. Bright, dense, and transient F-actin shells along the NE during NEBD have been observed in early embryos of diverse echinoderm species, including sea urchin, starfish, and sand dollars ([11] and our unpublished data). Thus, this mechanism is most likely required for mitosis in early embryos as well as oocytes, at least in echinoderms. Notably, in most other species, NEBD has not been characterized in such detail, and therefore it remains an open question whether this mechanism is conserved across other phyla.

Accession Numbers

The NCBI Nucleotide accession numbers for *Patiria miniata* alpha-actinin and Arpc1 reported in this paper are KJ787016 and KJ776755, respectively.

Supplemental Information

Supplemental Information includes Supplemental Experimental Procedures, four figures, and three movies and can be found with this article online at http://dx.doi.org/10.1016/j.cub.2014.05.019.

Acknowledgments

We would like to thank Jan Ellenberg and Nathalie Daigle (EMBL) for support in the early phase of the project and for comments on the manuscript. We thank Mark Terasaki (University of Connecticut Health Center) for his constant support throughout the project. We also thank Melina Schuh (MRC Laboratory of Molecular Biology) and Bill Bement (University of Wisconsin Madison) for comments on the manuscript. We would like to acknowledge the essential support of EMBL's Electron Microscopy Core Facility, specifically the help of Rachel Mellwig and Yannick Schwab. We thank Beáta Bugyi (University of Pécs) for providing purified tropomyosin and Arp2/3, Art Hand (University of Connecticut Health Center) for sharing EM protocols, and Patrick Leahy (Caltech) and Trevor Fay (Monterey Abalone) for supplying starfish animals. This research was funded by the EMBL and Deutsche Forschungsgemeinschaft (DFG) research grants SPP1464 EL 246/5-1 and LE 2926/1-1 to Jan Ellenberg and P.L., respectively. M.M. was additionally supported by the Uehara Memorial Foundation. N.M. and M.B. were supported by MIT Faculty Start-up Funds, and N.M. was additionally supported by a National Science Foundation Graduate Research Fellowship. Part of this work was performed at the Marine Biological Laboratory (Woods Hole).

Received: March 17, 2014
Revised: May 7, 2014
Accepted: May 8, 2014
Published: June 5, 2014

References

1. Burke, B., and Ellenberg, J. (2002). Remodelling the walls of the nucleus. Nat. Rev. Mol. Cell Biol. *3*, 487–497.
2. Güttinger, S., Laurell, E., and Kutay, U. (2009). Orchestrating nuclear envelope disassembly and reassembly during mitosis. Nat. Rev. Mol. Cell Biol. *10*, 178–191.
3. Hetzer, M.W. (2010). The nuclear envelope. Cold Spring Harb. Perspect. Biol. *2*, a000539.
4. Dultz, E., Zanin, E., Wurzenberger, C., Braun, M., Rabut, G., Sironi, L., and Ellenberg, J. (2008). Systematic kinetic analysis of mitotic dis- and reassembly of the nuclear pore in living cells. J. Cell Biol. *180*, 857–865.
5. Laurell, E., Beck, K., Krupina, K., Theerthagiri, G., Bodenmiller, B., Horvath, P., Aebersold, R., Antonin, W., and Kutay, U. (2011). Phosphorylation of Nup98 by multiple kinases is crucial for NPC disassembly during mitotic entry. Cell *144*, 539–550.
6. Lénárt, P., Rabut, G., Daigle, N., Hand, A.R., Terasaki, M., and Ellenberg, J. (2003). Nuclear envelope breakdown in starfish oocytes proceeds by partial NPC disassembly followed by a rapidly spreading fenestration of nuclear membranes. J. Cell Biol. *160*, 1055–1068.

7. Terasaki, M., Campagnola, P., Rolls, M.M., Stein, P.A., Ellenberg, J., Hinkle, B., and Slepchenko, B. (2001). A new model for nuclear envelope breakdown. Mol. Biol. Cell *12*, 503–510.
8. Beaudouin, J., Gerlich, D., Daigle, N., Eils, R., and Ellenberg, J. (2002). Nuclear envelope breakdown proceeds by microtubule-induced tearing of the lamina. Cell *108*, 83–96.
9. Mühlhäusser, P., and Kutay, U. (2007). An in vitro nuclear disassembly system reveals a role for the RanGTPase system and microtubule-dependent steps in nuclear envelope breakdown. J. Cell Biol. *178*, 595–610.
10. Lénárt, P., Bacher, C.P., Daigle, N., Hand, A.R., Eils, R., Terasaki, M., and Ellenberg, J. (2005). A contractile nuclear actin network drives chromosome congression in oocytes. Nature *436*, 812–818.
11. Burkel, B.M., von Dassow, G., and Bement, W.M. (2007). Versatile fluorescent probes for actin filaments based on the actin-binding domain of utrophin. Cell Motil. Cytoskeleton *64*, 822–832.
12. Riedl, J., Crevenna, A.H., Kessenbrock, K., Yu, J.H., Neukirchen, D., Bista, M., Bradke, F., Jenne, D., Holak, T.A., Werb, Z., et al. (2008). Lifeact: a versatile marker to visualize F-actin. Nat. Methods *5*, 605–607.
13. Mori, M., Monnier, N., Daigle, N., Bathe, M., Ellenberg, J., and Lénárt, P. (2011). Intracellular transport by an anchored homogeneously contracting F-actin meshwork. Curr. Biol. *21*, 606–611.
14. Nolen, B.J., Tomasevic, N., Russell, A., Pierce, D.W., Jia, Z., McCormick, C.D., Hartman, J., Sakowicz, R., and Pollard, T.D. (2009). Characterization of two classes of small molecule inhibitors of Arp2/3 complex. Nature *460*, 1031–1034.
15. Hetrick, B., Han, M.S., Helgeson, L.A., and Nolen, B.J. (2013). Small molecules CK-666 and CK-869 inhibit actin-related protein 2/3 complex by blocking an activating conformational change. Chem. Biol. *20*, 701–712.
16. Pollard, T.D. (2007). Regulation of actin filament assembly by Arp2/3 complex and formins. Annu. Rev. Biophys. Biomol. Struct. *36*, 451–477.
17. Ridley, A.J. (2011). Life at the leading edge. Cell *145*, 1012–1022.